

# The structural fitting and the interaction energy between the zeolite lattice models and organic molecules in the conversion of spirolactones to enones

A. Chatterjee<sup>a,\*</sup>, R. Vetrivel<sup>b</sup>, R. Sreekumar<sup>c</sup>, Y.V.S.N. Murthy<sup>c</sup>, C.N. Pillai<sup>c</sup>

<sup>a</sup> *Inorganic Material Section, Tohoku National Industrial Research Institute, AIST, 4-2-1 Nigatake, Miyagino-ku, Sendai 983, Japan*

<sup>b</sup> *Catalysis Division, National Chemical Laboratory, Pune 411 008, India*

<sup>c</sup> *Department of Chemistry, Indian Institute of Technology, Madras 600 036, India*

Received 20 January 1997; accepted 15 May 1997

## Abstract

We report here the results of our modeling studies and cluster calculations on the spirolactone to enone conversion reaction over zeolite catalysts. The structural role and the interaction energy introduced by the zeolite framework in this reaction are studied. The shape selective catalytic behavior of various zeolites are rationalized by comparing the dimension of the molecules and zeolite pore diameter. It is observed that the spirolactone and enone molecules have dynamic freedom to hop among the various sites inside the supercage of Zeolite-Y. The abstraction of proton at Bronsted acid site by ketonic oxygen of the reactant has been indicated as the first step in the reaction mechanism. The interaction energy of the molecules with the framework cluster and the electron redistribution occurring in the reactant molecules due to adsorption are brought out. These results are useful to understand the mechanism of the dehydration of spirolactones to form enones. © 1997 Elsevier Science B.V.

**Keywords:** Structural fitting; Interaction energy; Zeolite H-Y; Spirolactone; Enone; AM1

## 1. Introduction

The acyclic enones are important intermediates in the total synthesis of natural products and complex organic molecule [1–3]. The acid catalyzed intra molecular transformation of spirolactones over methanesulphonic acid — P<sub>2</sub>O<sub>5</sub> mixture is the conventional procedure [4,5]. The difficulties in working up and the

requirement of a large excess of the acid reagent are the drawbacks of the procedure. Recently, there has been reports wherein hazardous catalysts are replaced by environment-friendly zeolite catalysts for organic reactions [6–8]. In this background, Pillai and co-workers reported the application of various zeolite catalysts for the title reaction [9]. It was shown [10] that large amount of zeolites were required to adsorb all the reactant molecules for the successful conversion and the product could be obtained only by removal from the catalyst after the reaction using methanol.

\* Corresponding author. Fax: +81-22-2366839; e-mail: chatt@tniri.go.jp.

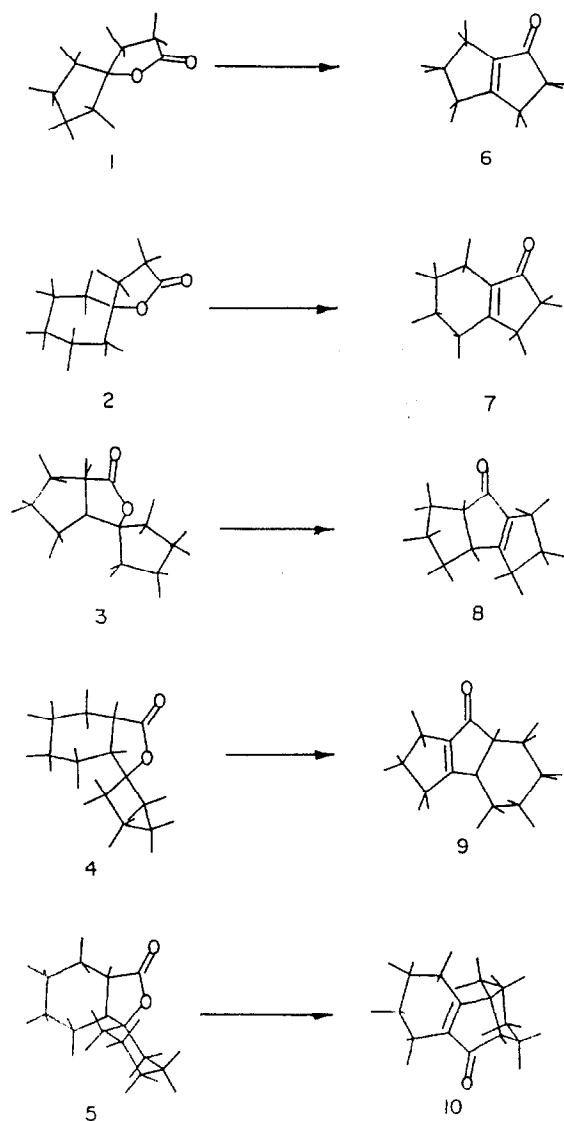


Fig. 1. The 3D structure of spirolactone and enone molecules, as derived from force field calculations.

In the present study, we apply computer simulation techniques to model the spirolactone to enone conversion. The structural relations between the spirolactone and the zeolite voids have been analyzed by molecular graphics and fitting techniques, which otherwise need to be determined by tedious experimental studies. The success of conversion of specific spirolactones (1–5) shown in Fig. 1 over zeolites with different pore architecture is analyzed. The reasons

for the requirement of ‘stoichiometric’ quantity of zeolites are probed. The mechanism of interaction of reactant and product molecules with the zeolite framework cluster models is studied by theoretical quantum chemical calculations. The interaction energy between the organic molecules (1–10) shown in Fig. 1 and the zeolite H–Y host lattice are studied to understand the mechanism of conversion reaction.

## 2. Methodology

The equilibrium geometry of the reactant and product molecules shown in Fig. 1 were obtained by force field calculations developed by Gelin and Karplus [11]. The total strain energy of the molecule is expressed by the following equation:

$$E_{\text{total strain}} = E_{\text{bonded}} + E_{\text{non-bonded}} \quad (1)$$

where

$$E_{\text{bonded}} = E_{\text{bond length}} + E_{\text{bond angle}} + E_{\text{dihedral angle}} + E_{\text{improper torsion}} \quad (2)$$

$$E_{\text{non-bonded}} = E_{\text{electrostatic}} + E_{\text{Van der Waals}} \quad (3)$$

The respective expressions used to calculate the individual terms are given in our earlier studies [12]. The visualization and calculations of energy were performed using Quanta/CharmM software packages distributed by Polygen Corporation, U.S.A.. The strain energy of the molecule was minimized as a function of geometry by the Steepest Descent method to eliminate initial bad contacts and then later by the Conjugate Gradient and Newton–Raphson methods.

The H–Y lattice was modeled from the structure reported by X-ray crystallographic studies [13]. The semi-empirical quantum chemical method using AM1 Hamiltonian [14] is adopted to perform the cluster calculations using the AMPAC code (QCPE Program No. 539).

### 3. Results and discussion

#### 3.1. The importance of the void dimensions in zeolites

The reactant and product molecules were shown as molecular graphics pictures. Their 3-dimensional equilibrium conformations corresponding to the minimum strain energy were obtained with well-established force field methods [11] and their realistic 3-dimensional conformations are shown in Fig. 1. Breck [15] had initiated a convention of reporting the kinetic diameter of a molecule as the intermolecular distance at the closest approach of two molecules. Recently, there are phenomenal advances in molecular graphics techniques. Hence, more accurate information regarding the size, namely the three largest dimensions of the molecules could be provided. Assuming that the molecules are exactly fitting inside a smallest possible rectangular box, the dimensions of the molecules are the dimensions of the box (Fig. 2) as shown in Table 1. In Table 1, the dimensions of the intermediates (11–15) formed from the reactants (1–5) according to the proposed mechanism in Scheme 1 are also included.

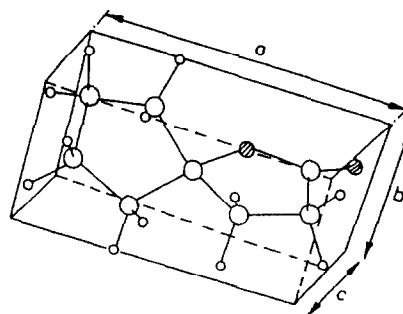


Fig. 2. The three largest dimensions of the molecule as used in the molecular fitting procedures. Spirolactone (1) is shown as a typical example. Shaded circles, large empty circles and small empty circles are respectively oxygen, carbon and hydrogen atoms.

The product molecules (6–10) are of similar or smaller dimensions than the reactant molecules (1–5). It is convention to neglect the largest dimension of the molecule, since the molecules can diffuse into the channels and cages with their largest dimension lying parallel to the channel axis. The intermediate molecules have more conformational flexibility. In general, the intermediates occupy more space and have less strain energy. In contrast, the product molecules occupy less space with more strain energy. In Table 1, we report the strain energy due to bonded and non-bonded interactions. The

Table 1

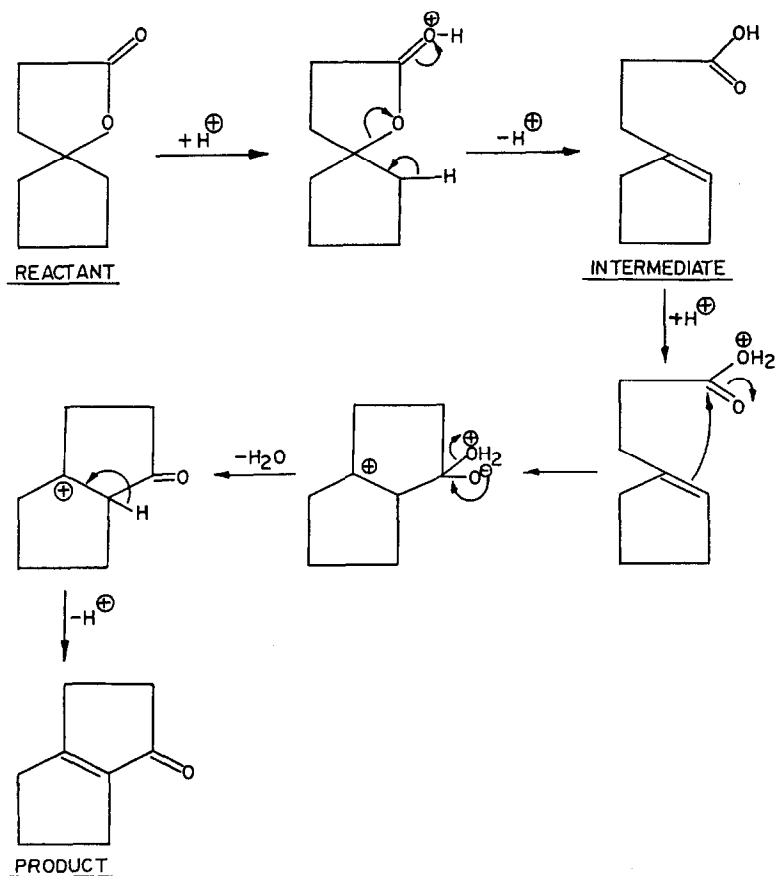
Total strain energy and dimensions of various molecules at their minimum energy configuration. The number of molecules are as assigned in Fig. 1, 11 to 15 are the intermediates formed from the spirolactones 1 to 5, respectively, according to the mechanism shown in Scheme 1

Molecule	No. of atoms	Dimension (Å)	Strain energy (kcal/mol)		
			total	bonded	nonbonded
1	22	7.00 × 4.25 × 4.00	15.7889	21.5913	−5.8035
2	25	7.00 × 4.25 × 4.25	6.4875	10.2886	−3.8035
3	29	7.50 × 5.50 × 5.50	20.8836	21.8529	−0.9693
4	32	7.50 × 6.00 × 6.00	19.8921	24.8102	−4.9182
5	35	7.75 × 5.65 × 5.65	8.5793	12.3631	−3.7837
11	22	6.25 × 5.25 × 5.00	2.1288	14.2986	−12.1699
12	25	7.25 × 5.25 × 5.25	−10.9613	2.0318	−12.9931
13	29	7.00 × 5.50 × 5.50	17.1363	25.7821	−8.6458
14	32	7.00 × 5.75 × 5.70	5.0534	15.5062	−10.4528
15	35	8.25 × 5.85 × 5.85	−5.5627	3.9035	−9.4662
6	19	6.50 × 4.50 × 4.50	17.8080	19.9514	−2.1435
7	22	6.00 × 4.65 × 4.65	15.6723	15.6289	0.0434
8	26	6.75 × 5.10 × 5.10	27.7583	30.1872	−2.4270
9	29	7.10 × 5.50 × 5.50	21.7622	24.8070	−3.0447
10	32	8.00 × 5.25 × 5.25	21.7622	17.8135	0.7447

analysis of the individual contributions of various bonded and non-bonded terms to the strain energy of these molecules were discussed in our earlier report [16]. Non-bonded energy arises from electrostatic and Van der Waals interactions. Favorable and unfavorable non-bonded term arises due to the attraction between polar groups with unlike charges and repulsion between polar groups with like charges respectively. Here we bring out the point that the bonded energy terms are unfavorable, while the non-bonded energy terms are favorable as indicated by almost zero or negative values. Compared to the reactants, intermediates have favorable non-bonded energy and products have unfavorable non-bonded energy. Thus, relatively unfavorable non-bonded energy for product molecules indicate the presence of positively

charged groups in the molecule. These results indicate that the positive charges in the molecules have ionic interaction with the oxygens of the zeolite framework, which could lead to their stronger adsorption inside the zeolite void volumes. The reactant and intermediate molecules have both positive and negatively charged atoms/groups. This is in correspondence with the experimental finding [10] that the final product had to be solvent extracted after the reaction.

The pore diameters of various zeolites are known from the reported crystal structures [17]. It is possible to study the fitting of different molecules in several zeolites. The product yields of enones over different zeolites obtained in the experimental study [10] are given in Table 2. The yields of enones (6–10) over various zeo-



Scheme 1.

Table 2

The yield of various enones over different zeolites [10]. (Temperature = 150°C, time = 6 h, amount of catalyst = 5.0 g, amount of substrate = 0.5 g, solvent = hexane)

Catalyst	Yield of enones (mol%)				
	(6)	(7)	(8)	(9)	(10)
H-ZSM-5	69	61	0	0	0
H-ZSM-12	79	68	0	0	0
H-Beta	77	70	52	58	56
H-EMT	84	78	64	66	68
H-Y	92	95	90	89	86

lites which are listed in Table 2 could be rationalized from the pore diameters of the zeolites. H-ZSM-5 has 2D channels with diameters of 5.1 Å and 5.4 Å, while H-ZSM-12 has 1D elliptical channel of diameters 5.7 Å and 5.9 Å. H-Beta has 2D channels with diameters 6.5 Å and 7.5 Å. H-EMT and H-Y has large supercages with elliptical (7.1 Å × 7.4 Å) and circular (7.4 Å) windows respectively opening into the supercages. These results are illustrated in Fig. 3. The linear bicyclic lactones (1 & 2) are small enough to enter the medium pores of H-ZSM-5 as well as large pores of H-ZSM12, H-Beta, H-EMT and H-Y. However, the tricyclic lactones, such as 3, 4 & 5 are having an angular conformation. They can not diffuse into the channels of H-ZSM-5 and H-ZSM12. Thus the product yields of various enones obtained

over different zeolite catalysts are in correspondence with their structural fitting. It can be generalized that large pore zeolites with cage structures are efficient catalysts for this conversion. Thus the role of shape selectivity in controlling the yield are commonly brought out from these results.

### 3.2. The importance of interaction energy

Although the void dimensions of the zeolite catalysts control the product yield, the electronic interactions are also expected to play a vital role in the mechanism of this conversion reaction. The typical results of experimental findings for the formation of enone (8) from spirolactone (3) at 150°C for 6 h are given in Table 3. The results show that the yield obtained is dependent on the solvent media as well as on the amount of catalyst used. It is observed that with the same amount of catalyst and reactant (comparing the experiments 1 & 2), the yield decreases for a polar solvent like methanol. When the amount of catalyst is reduced, the number of supercages as well as the catalyst surface available for the reactants decrease. This leads to a drastic decrease in the product yield (compare the experiments 1 and 5 in Table 3) for a given reaction. In experiment 5, the cata-

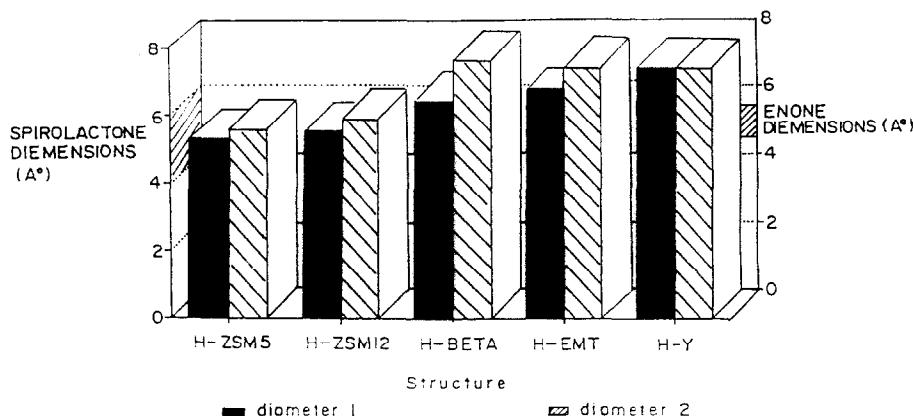


Fig. 3. The schematic representation of the pore diameters in various zeolites used as catalysts. The diameters of two pores in case of 2D pore structures or the two diameters of elliptical 1D pore structures are shown. The range of smallest dimension of the reactant spirolactone and product enone molecules are indicated as shaded regions. The actual dimensions are given in Table 1.

Table 3

Comparison of the yield of enone (8) over Zeolite H–Y at various reactant/catalyst weight ratios. The effect of different solvents on the final product yield is also shown [9]. (Temperature = 150°C, time = 6 h)

No.	Weight of catalyst (g)	No. Super of cages	Weight of reactant (g)	No. reactant molecules	Reactant/catalyst weight ratios	Solvent	Yield (%)
1.	10.0	$1.0 \times 10^{21}$	1.0	$3.6 \times 10^{21}$	0.10	H	90
2.	10.0	$1.0 \times 10^{21}$	1.0	$3.6 \times 10^{21}$	0.10	M	19
3.	5.0	$5.0 \times 10^{20}$	0.5	$1.8 \times 10^{21}$	0.10	M:H(1:4)	58
4.	0.2	$2.0 \times 10^{19}$	1.0	$3.6 \times 10^{21}$	5.00	M:H(1:4)	8
5.	0.1	$1.0 \times 10^{19}$	1.0	$3.6 \times 10^{21}$	10.00	H	< 1

M = Methanol, H = Hexane.

lyst amount is reduced to 1/100th of the amount of experiment 1, while keeping all the experimental conditions same. The product yield decreased from 90% to less than 1%. However, the adsorption of molecules on the external surface is expected to be weak compared to that inside the cage. Hence, the active sites on the surface will be easily replenished, compared to those sites inside the cages. The results indicate that there is a direct correlation between the number of super cages and the product yield. Additionally, if the reaction occurs on the surface, stoichiometric amount of catalyst will not be required as in the case in our study. Thus the results in Table 3 indicate that the present reactions are occurring inside the cages and not on

the catalyst surfaces. Further, polar solvents such as methanol led to low conversion. This may be due to competitive adsorption of methanol or due to catalyst deactivation by methanol. Thus the interaction energy of molecules with the zeolite framework due to the presence of polar groups is also important in addition to shape selective behavior of zeolites. The solvent effect is complicated and its difficult to probe it with computational techniques at this stage. However, we studied the adsorption mode of the molecules inside the supercage of H–Y and the mechanism of electron transfer between organic molecules and the framework of zeolite H–Y by AM1 calculations.

The total energy of the reactant, proposed

Table 4

Electronic properties of reactants, intermediates and products

Molecule	Total energy (eV)	Charge on oxygen		Bond order between C and O	
		ring	ketonic	ring	ketonic
1	-1829.25	-0.28	-0.32	0.934	1.857
11	-1831.24	-0.28	-0.31	0.954	1.869
6	-1481.28	...	-0.28	...	1.868
2	-1986.88	-0.24	-0.30	0.923	1.831
12	-1987.31	-0.26	-0.30	0.933	1.857
7	-1637.71	...	-0.29	...	1.883
3	-2270.42	-0.23	-0.30	0.924	1.825
13	-2270.66	-0.25	-0.29	0.936	1.858
8	-1920.73	...	-0.28	...	1.866
4	-2426.12	-0.23	-0.30	0.923	1.826
14	-2426.70	-0.25	-0.30	0.936	1.857
9	-2076.03	...	-0.28	...	1.866
5	-2582.01	-0.24	-0.30	0.923	1.832
15	-2582.75	-0.26	-0.31	0.933	1.872
10	-2232.75	...	-0.29	...	1.884

intermediates (according to Scheme 1) and the product molecules are given in Table 4. The total energy values are in the order: product + water > reactant > intermediate.

These results are in correlation with those obtained from force field calculations (Table 1). The net charges calculated from Mulliken Population analysis indicate that the ketonic oxygens are more negative than the ring oxygens. Hence the ketonic oxygen atoms are expected to have interaction with the proton of the Bronsted acid site of zeolite. The bond order of C–O bond in the ring as well as ketonic group are also given in Table 4. The variation C–O bond in the ring during the interaction with the zeolite framework is discussed in the following section.

Since H–Y was found to give the best yield (Table 2) and the structural fitting is also the most favorable for zeolite Y among all the zeolites used, we studied in detail the interaction of molecules with H–Y framework. The 12-member pore opening in Zeolite H–Y has

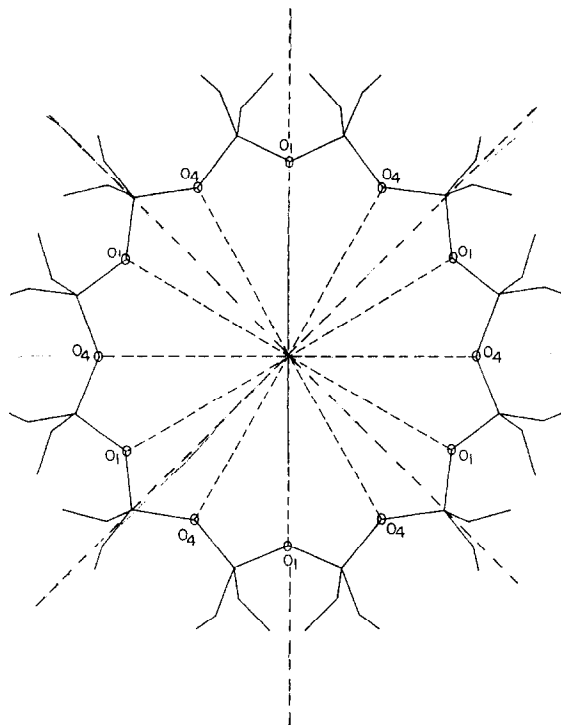


Fig. 4. The molecular graphics view of the 12-member ring pore opening in zeolite H–Y as viewed along the 'b' axis.

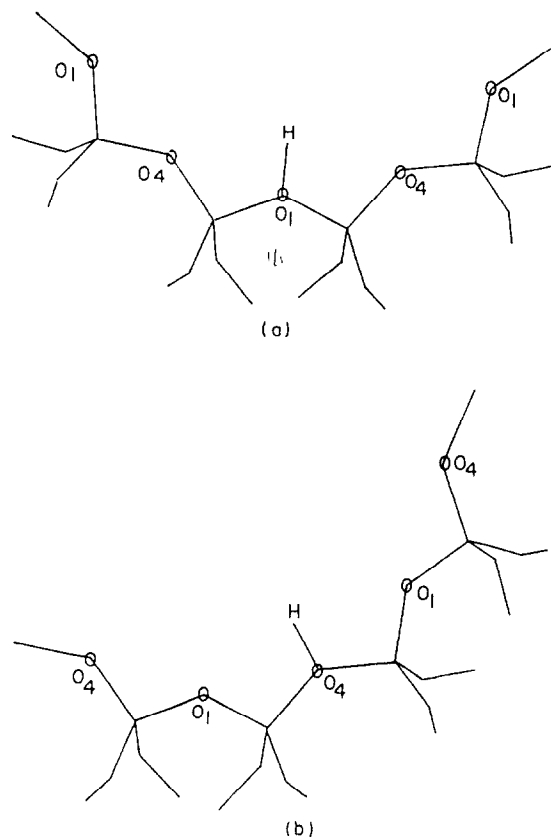


Fig. 5. The tetrameric cluster centered at O<sub>1</sub> (FWC1) and O<sub>4</sub> (FWC4) of zeolite H–Y framework are shown as structures (a) and (b), respectively. These cluster models represent the two possible Bronsted acid sites in 12 m ring of H–Y.

$C_{6v}$  symmetry along the pore opening as shown in Fig. 4 although the 12-membered ring itself is puckered one. Two tetrameric clusters, each of them centered at O<sub>1</sub> and O<sub>4</sub> are considered to represent two possible interaction sites in faujasite. These tetrameric clusters consist four T-sites linked to each other by a bridging oxygen and they are one-third fragment of the 12-member ring. The Si/Al ratio of H–Y zeolite catalyst used was 2.6. Therefore, as the nearest approximation we have substituted one of the four Si<sup>4+</sup> by Al<sup>3+</sup> and the anionic charge of the framework is compensated by a proton on the bridging oxygen. The proton is located in the 12-m ring. The stoichiometry of the clusters are H<sub>11</sub>Si<sub>3</sub>AlO<sub>13</sub> and their actual configurations are shown in Fig. 5a and b. The electronic proper-

ties of these cluster models representing the H–Y faujasite framework were calculated and given in Table 5. The net charges on  $O_4$  ( $-0.56$ ) and  $O_1$  ( $-0.58$ ) in these clusters are almost same in accordance with their similarity in geometry: T– $O_1$ –T and T– $O_4$ –T angles are  $135.38^\circ$  and  $136.27^\circ$ , respectively and T– $O_1$  and T– $O_4$  are  $1.68 \text{ \AA}$  and  $1.69 \text{ \AA}$ , respectively.

The interaction of organic molecules with these cluster models are studied. The adsorption complex formed between the molecule and the zeolite is simulated by a cluster model. The cluster model is created by fitting the molecule inside the supercage of H–Y [16]. The two criteria considered were that there should be interaction between the Bronsted acid site and ketonic oxygen, as well as the orientation should not lead to any bad contacts between the Van der Waals radii of atoms in the molecule and the zeolite framework. The conformation of the

adsorption complexes between zeolite framework cluster and spiro lactone (1) as well as enone (6) are shown as typical examples in Fig. 6a and b respectively. The interaction energy between the molecule and the framework cluster given in Table 5 are calculated according to the relation given in Eq. (4):

$$\text{Interaction energy} = \text{Total energy of complex} - [\text{Total energy of framework} + \text{Total energy of molecules}] \quad (4)$$

As for the cluster centered at  $O_1$  (Fig. 5a) and  $O_4$  (Fig. 5b), the organic molecules are found to have multi-site interaction with the framework. In the ‘zeolite cluster: organic molecule’ complex, it was found that the major interaction was between the methylene hydrogen of the organic molecule and the oxygen of framework. The net charges calculated by Mulliken Population anal-

Table 5

Interaction energy of reactants and products with framework cluster centered on the Oxygen site  $O_1$  and  $O_4$ . FWC1 and FWC4 are shown in Fig. 5a and b respectively

Molecule	Total energy (eV)	Interaction energy (eV)	Charge on oxygen		Bond order between C and O in the ring
			ring	ketonic	
Cluster centered at $O_1$ (FWC1)	-4588.55	...	...	...	...
Cluster centered at $O_4$ (FWC4)	-4588.39	...	...	...	...
Water molecule	-348.56	...	...	...	...
FWC1 + 1	-6417.67	0.13	-0.28	-0.31	0.933
FWC4 + 1	-6417.62	0.12	-0.26	-0.34	0.922
FWC1 + 2	-6575.15	0.28	-0.25	-0.26	0.922
FWC4 + 2	-6574.86	0.41	-0.26	-0.22	0.922
FWC1 + 3	-6858.86	0.11	-0.23	-0.29	0.919
FWC4 + 3	-6858.73	0.07	-0.21	-0.31	0.920
FWC1 + 4	-7014.41	0.26	-0.24	-0.27	0.922
FWC4 + 4	-7014.12	0.38	-0.25	-0.23	0.920
FWC1 + 5	-7170.35	0.20	-0.24	-0.28	0.922
FWC4 + 5	-7169.72	0.67	-0.26	-0.21	0.921
FWC1 + 6	-6069.86	-0.03	...	-0.26	...
FWC4 + 6	-6069.55	0.01	...	-0.28	...
FWC1 + 7	-6226.30	-0.04	...	-0.29	...
FWC4 + 7	-6226.05	0.08	...	-0.29	...
FWC1 + 8	-6509.29	-0.01	...	-0.29	...
FWC4 + 8	-6509.05	0.07	...	-0.29	...
FWC1 + 9	-6664.45	0.13	...	-0.25	...
FWC4 + 9	-6664.39	0.09	...	-0.28	...
FWC1 + 10	-6821.36	-0.07	...	-0.29	...
FWC4 + 10	-6821.09	0.04	...	-0.29	...

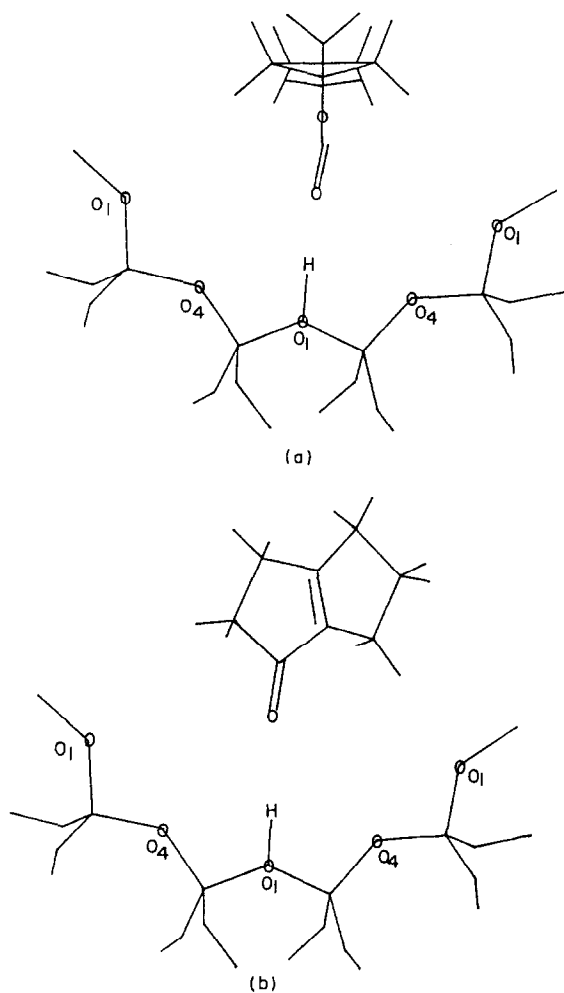


Fig. 6. The orientation of a typical spirolactone (1) and enone (6) molecules with respect to the zeolite framework cluster model shown in Fig. 5a. These cluster models are chosen to study the electronic interaction between the molecule and zeolite framework.

ysis (Table 5) show that the product molecules are more polar than the reactant molecules. Consequently, the interaction energy of the enones with the framework are relatively favorable than the spirolactones.

Similar calculations were performed for the cluster centered at  $O_4$ . The geometric features such as T–O and T–O–T around  $O_1$  and  $O_4$  are almost same as discussed above. Consequently, the total energy and other electronic properties calculated for the adsorption complexes of molecules with cluster models centered at  $O_4$

were close as well as following the same trend as for the cluster centered at  $O_1$ . Thus, it was evident that there are several isoenergy sites for the activation of molecules inside the supercage.

Much importance can not be laid on the actual numerical values due to confined cluster models. However, the qualitative trends predicted for the interaction of various molecules will be reliable. Chemically, the conversion of spirolactones to enones is a dehydration process. The solvation by water molecules as well as their interaction with the framework of hydrophilic zeolites such as H–Y are poorly understood phenomena. In spite of these complications, comparison of the electronic properties of free and adsorbed molecules given in Tables 4 and 5, respectively show some small but subtle changes. The bond order of C–O bond in the ring shows a slight decrease due to adsorption, indicating the tendency for weakening. Indeed, geometry optimization calculations would be needed to simulate the realistic bond fission process taking place. The net negative charges on the oxygen in the rings remain constant or there is a slight increase, whereas the negative charge on the ketonic oxygen decreases. The ketonic oxygen atoms in the product molecules have lesser negative charge than the reactant molecules. Thus the electron redistribution predicted by the present calculations indicate that the ketonic oxygen of the reactant molecules abstract the proton from Bronsted acid site, although the ring oxygen is removed during dehydration. Thus the results support the mechanism proposed in Scheme 1.

#### 4. Conclusions

The use of zeolite catalysts in place of conventional acid catalyst has been demonstrated for the conversion of spirolactones to enones. The zeolite catalysts have obvious advantages and far reaching consequences, such as recycling of the catalyst and easy working up. The yields obtained in the conversion of several

spirolactones to enones are in correspondence with the structural fitting of these molecules inside zeolite channels or cages. Thus the shape selective catalytic behavior of various zeolites have been rationalized and some generalizations have been derived.

The interaction energy of the products with the zeolite framework are more favorable than the interaction energy of reactants with the framework. Thus the final products formed have to be solvent extracted otherwise the cages are not available for other reactants. Hence stoichiometric quantity of zeolite catalysts are required in the reaction. The comparison of electronic properties of the free and adsorbed organic molecules at their minimum energy conformations are useful to understand the mechanism of conversion.

The applicability of computer modeling studies has been established for this reaction; given a new spirolactone reactant, the feasibility of its conversion to enones over a zeolite catalyst can be predicted. The general computer simulation technique can be applied to study several other organic reactions catalyzed by zeolites.

## References

- [1] M. Karpf, A.S. Dreiding, *Helv. Chim. Acta* 64 (1981) 1123.
- [2] P.E. Eaton, *Tetrahedron* 37 (1981) 4479.
- [3] Y.V.S.N. Murthy, C.N. Pillai, *Tetrahedron* 48 (1992) 5331.
- [4] P.E. Eaton, G.R. Carlson, J.T. Lee, *J. Org. Chem.* 38 (1973) 4071.
- [5] Y.V.S.N. Murthy, C.N. Pillai, *Tetrahedron Lett.* 31 (1990) 6067.
- [6] C.R. Mordi, R. Fields, J. Dwyer, *J. Mol. Catal.* 92 (1994) 51.
- [7] U. Kameswari, C.S. Swami, C.N. Pillai, *Stud. Surf. Sci. Catal.* 84 (1994) 1959.
- [8] M. Ziolk, P. Decyk, *Stud. Surf. Sci. Catal.* 84 (1994) 1579.
- [9] R. Sreekumar, Y.V.S.N. Murthy, C.N. Pillai, *J. C. S. Chem. Commun.* 1624 (1992).
- [10] R. Sreekumar, Y.V.S.N. Murthy, C.N. Pillai, in: P. Kanta Rao, R.S. Beriwal (Eds.), *Catalysis: Present & Future*, Wiley Eastern, New Delhi, 1995, p. 99.
- [11] B.R. Gelin, M. Karplus, *Biochemistry* 18 (1979) 1256.
- [12] B.M. Bhawal, R. Vetrivel, T.I. Reddy, A.R.A.S. Deshmukh, S. Rajappa, *J. Phys. Org. Chem.* 7 (1994) 377.
- [13] D.H. Olson, *J. Phys. Chem.* 74 (1970) 2758.
- [14] M.J.S. Dewar, E.G. Zoebisch, E.F. Healy, J.J.P. Stewart, *J. Am. Chem. Soc.* 107 (1985) 3902.
- [15] D.W. Breck, *Zeolite Molecular Sieves: Structure, Chemistry and Use*, Wiley, New York, 1974, p. 634.
- [16] A. Chatterjee, R. Vetrivel, R. Sreekumar, Y.V.S.N. Murthy, C.N. Pillai, in: N.M. Gupta, D.K. Chakraborty (Eds.), *Catalysis: Modern Trends*, Narosa Publishing House, New Delhi, 1996, p. 68.
- [17] W.M. Meier, D.H. Olson, *Atlas of Zeolite structure types, Zeolites*, Butterworth-Heinman, London, 1992.